Laminar flow of a viscoelastic shear-thinning liquid over a backward-facing step preceded by a gradual contraction

R. J. Poole and M. P. Escudier
Department of Engineering, University of Liverpool, Brownlow Hill, Liverpool L69 3GH, United Kingdom

A. Afonso
*Centro de Estudos de Fenómenos de Transporte, DEMEGI, Faculdade de Engenharia,
Universidade do Porto, Rua Dr. Roberto Frias s/n, 4200-465 Porto, Portugal*

F. T. Pinho
*Centro de Estudos de Fenómenos de Transporte, Faculdade de Engenharia, Universidade do Porto,
Rua Dr. Roberto Frias s/n, 4200-465 Porto, Portugal and Universidade do Minho, Largo do Paço,
4704-553 Braga, Portugal*

Experimental observations and numerical simulations, based upon the Phan-Thien and Tanner model, are reported for the laminar flow of a series of viscoelastic liquids (0.05%, 0.1%, and 0.4% concentrations of a polyacrylamide) over a symmetrical, double backward-facing step geometry preceded by a short gradual contraction from a long (120 hydraulic diameters in length) square duct. Reynolds numbers are typically between 10 and 100 (i.e., inertia is not negligible) and Deborah numbers of order 100 for the experiments (based on a relaxation time determined from linear viscoelasticity measurements) and order 10 for the viscoelastic simulations. As the polymer concentration is increased, the combined effects of increased shear thinning and viscoelasticity are found to dramatically reduce the length of the recirculation region downstream of the step. The nature of the flow field within the contraction itself is found to be fundamentally different for the viscoelastic liquids to that for a comparable Newtonian fluid flow: large velocity overshoots with very strong gradients appear near to the sidewalls that, due to their appearance, we have dubbed "cat's ears." The simulations are able to reproduce these remarkable features, at least qualitatively. © 2007 American Institute of Physics. [DOI: 10.1063/1.2769380]

I. INTRODUCTION

For laminar flow of a Newtonian fluid through a plane sudden expansion, it is well known that above a critical Reynolds number for an expansion ratio (R=duct height downstream of expansion/duct height upstream of expansion $=D/d$) greater than 1.5, the flow field downstream of the expansion develops stable top-to-bottom asymmetry (the rectangular inlet to the expansion is regarded as having a horizontal orientation: a convention we adopt throughout this paper). This asymmetry has been observed both experimentally[1–3] and numerically.[4,5] For non-Newtonian fluid flows the extent of the available data is much more limited, especially so far as quantitative experimental data are concerned, and the data have been discussed in a recent paper.[6] In that paper experimental observations were reported for the flow of a 0.05% by weight polyacrylamide solution through a plane sudden expansion of expansion ratio 4 and aspect ratio (A=width of duct/step height=w/h) 5.33. As is also the case in the study reported here, the plane sudden expansion was preceded immediately by a short gradual contraction from a long (120 hydraulic diameters in length) square duct. In contrast to the flow of a Newtonian fluid, downstream of the expansion the top-to-bottom asymmetry was greatly reduced, with very similar reattachment lengths for the two recirculation regions. More significantly, the flow unexpectedly developed a strongly three-dimensional jet-like structure, with side-to-side symmetry centered on the "vertical" symmetry plane of the contraction/expansion geometry. For the viscoelastic liquid, the flow field within the contraction itself was also observed to be fundamentally different from that for the flow of a Newtonian fluid at a comparable Reynolds number. Large velocity overshoots with very strong gradients developed near the sidewalls that, due to their appearance, Poole *et al.*[6] dubbed "cat's ears." The fully developed approach flow in the square duct was unremarkable and it was speculated that the cat's ears effect was a consequence of the large normal-stress differences that arise in highly viscoelastic liquids. These remarkable features, hitherto unreported, motivated the current study in which the only difference to the previous work is that the gradual-contraction/sudden-expansion geometry has a lower contraction/expansion ratio of 8:2.3 (contraction) and 1:1.43 (expansion). Guided by experience with Newtonian fluid flow, this particular expansion ratio was selected with the intention of avoiding the possibility of top-to-bottom asymmetry so that one half of the geometry can be regarded as a backward-facing step. In the work reported here, a range of polyacrylamide concentrations has been investigated experimentally and we have also conducted a series of inelastic and viscoelastic numerical simulations, the latter based on the Phan-Thien and Tanner (PTT) model, in an attempt to identify the physical mechanisms responsible

for the cat's-ears phenomenon and their ability to predict the flow field downstream of the backward facing step.

For expansion ratios below 1.5 the flow downstream of plane sudden expansions, for Newtonian fluids at least, remains symmetric and the geometry behaves essentially as a double backward-facing step. The recent paper by Biswas *et al.*[7] provides a succinct review of the extensive literature for laminar flow of a Newtonian fluid over a backward-facing step. The flow field downstream of a backward-facing step, or indeed any sudden-expansion geometry (axisymmetric or planar), can be characterized by five elements; a central core, a free shear layer, a recirculation region (at sufficiently high Reynolds numbers at least), a corner eddy, and a developing boundary layer. As the flow enters the expansion it is unable to negotiate the abrupt nature of the step and separates from the wall [at very low Reynolds numbers ($\leqslant 1$) the flow does not separate from the expansion] but there is a recirculation located in the re-entrant corner known as a Moffat vortex.[7,8] The boundary layer of the inlet flow develops into a free shear layer that grows with streamwise distance due to a transverse transfer of streamwise momentum. Bounded between this free shear layer and the duct centerline is a high-velocity core which originates from the free stream of the inlet flow. The region between the free shear layer and the wall is a region of intense recirculation, embedded within which is a small counter-rotating corner eddy. At a sufficient distance downstream the free shear layer reattaches to the wall (the so-called reattachment point) and a new boundary layer develops. While the flow remains laminar, the length of this recirculation region increases approximately linearly with Re.

In contrast to the situation for Newtonian fluids, for the flow of non-Newtonian fluids the available literature is restricted to two papers: the purely numerical work of Hsu and Chou,[9] who conducted time-dependent, two-dimensional simulations of the flow of second-order fluids over a backward facing step, and the experimental study of Gijsen *et al.*[10] who measured the wall shear stress distribution behind a step for a red blood cell suspension but reported no details of the flow field. Using first order in time and second order in space discretizations, Hsu and Chou reported a decrease in the recirculation due to fluid elasticity and enhancement of elastic effects by inertia. As we have already mentioned, in the present study the expansion ratio is 1.43 and we shall henceforth refer to the flow geometry as a backward-facing step rather than as a plane sudden expansion in recognition of the inherent symmetry of the flow field which was confirmed by our observations.

So far as viscoelastic fluid flows through plane sudden expansions are concerned the literature is again rather scarce. Townsend and Walters[11] used flow visualization to observe the laminar flow field downstream of both a two-dimensional and a three-dimensional expansion for aqueous solutions of a polyacrylamide (0.15%), a xanthan gum (0.1%) and a glass fiber suspension (0.025%). The conclusion drawn from their study was that the viscoelasticity of the polymer solutions damped out the vortex activity and caused any recirculating fluid to be pushed into the corners of the expansion. They used the "linear" form of the Phan-Thien and Tanner (PTT)
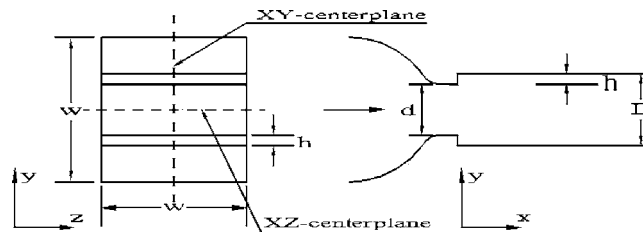

FIG. 1. Double backward-facing step geometry.

model[12] in an attempt to simulate the viscoelastic behavior of the polyacrylamide solution. The PTT simulation ($\varepsilon = 0.02$, Re$= \rho . UL/\eta_0 = 10$ and We$= \lambda . U/L = 1$, where U and L are characteristic velocity and length scales, η_0 is the sum of the solvent and polymer viscosities and λ is the relaxation time) produced results in good qualitative agreement with the flow visualization. The experiments of Townsend and Walters[11] were also used as the basis for comparison in the numerical simulation work of Baloch *et al.*[13] who modelled expansion flows in two and three dimensions, again using the linear form of the PTT model. Once again good qualitative agreement with the experimental visualizations was found and the conclusion again drawn that viscoelasticity suppresses vortex activity and that this suppression is linked to the phenomenon of extrudate swell.

The series of experiments reported in the current paper was guided by our observations of the complex nature of the flow field within the gradual contraction, albeit for different gradual contraction/expansion ratios, reported in Poole *et al.*[6] As a consequence, measurements were taken both in the approach flow in the square duct, within the gradual contraction and downstream of the step. As will become apparent, despite the large differences in area contraction ratio between the two studies (2.86:1 in the current study compared to 8:1 in Poole *et al.*[6]), the remarkable flow features, which we dubbed cat's ears, are again found to be present. The appearance of off-centerline phenomena in viscoelastic flows is not new: the experiments of Lee *et al.*[14] with polymer melts in a multipass rheometer have shown off-center stress maxima (called stress "fangs"). However these maxima occurred as a consequence of the different strain histories experienced by fluid particles starting their flow in the slit and particles starting their flow in the upstream duct. These maxima were observed only during the transient startup phase of the motion and disappeared as the flow reached steady state in marked contrast to the steady-state phenomena reported here.

II. EXPERIMENTAL RIG AND INSTRUMENTATION

The flow loop used for the present experiments is identical to that used by Poole *et al.*[6] and is a modified version of that used by Escudier and Smith[15] for their square-duct investigation. The square duct consisted of ten stainless steel modules each of length 1.2 m with an internal cross section of side length $w = 80$ mm. The double backward-facing step, for which the key dimensions are given in Fig. 1, was located 9.6 m downstream of the inlet connection to the square duct. This arrangement provides a length of 120 hydraulic diameters for the approach flow to become fully developed. The

expansion was preceded by a short (50 mm length), gradual, plane contraction (50 mm concave radius followed by 11 mm convex radius). The duct width w throughout (including the contraction) was 80 mm, the inlet height at exit from the contraction d was 28 mm, and the step height h was 6 mm. The height D of the downstream rectangular duct following the expansion was 40 mm. The sidewalls of the contraction, the downstream duct and the square duct just upstream of the contraction were all made of borosilicate glass to permit velocity measurements using a laser Doppler anemometer (LDA). For the two low-concentration (0.05% and 0.1%) solutions of PAA (the rheology of all working fluids is discussed in Sec. III), distributions of streamwise velocity (U) were obtained within the XY-centerplane from vertical traverses (i.e., in the y-direction) at 10 streamwise locations within the downstream duct corresponding to x/h values of 0, 1, 2, 3, 4, 5, 6, 7, 8, and 10. More limited measurements are reported for 0.4% PAA at x/h values of 0, 1, 2, 3, 4, 6, and 10. Distributions of streamwise velocity were also obtained from horizontal traverses across the duct (i.e., in the z-direction along $y/w=0$) within the XZ-centerplane both within the contraction ($x/h=-7$) and at the inlet to the backward-facing step (i.e., $x/h=0$). For the highest (0.4%) and lowest (0.05%) PAA concentrations the approach flow within the square duct was mapped at a streamwise location approximately 240 mm (i.e., 3 hydraulic diameters of the square duct) upstream of the gradual contraction by measuring distributions of streamwise velocity along horizontal traverses at $y/w=0$, 0.125, 0.25, and 0.375 and along a vertical traverse at $z/w=0$.

A Dantec Fibreflow laser Doppler anemometer system was used for the velocity measurements and was comprised of a Dantec 60×10 probe and a Dantec 55×12 beam expander in conjunction with a Dantec Burst Spectrum Analyzer signal processor (model 57N10). The beam separation at the front lens was 51.5 mm and the lens focal length 160 mm which produced a measurement volume in water with principal axis of length 0.21 mm and diameter 20 μm. Ensemble averages at each measurement location were formed from not less than 9500 velocity samples. The total uncertainty in the mean velocity values is estimated to be in the range 3%–4%.[16]

The bulk flow rate $\dot{Q}_F$ was measured using a Fischer and Porter electromagnetic flowmeter (model 10D1) incorporated in the flow loop upstream of the square duct with the flowmeter output signal recorded via an Amplicon PS 30AT A/D converter.

All rheological measurements were carried out using a TA Instruments Rheolyst AR 1000N controlled-stress rheometer with the liquid sample at a temperature of 20 °C, which was also the average temperature of the fluid within the flow loop for the duration of the experimental runs. Temperature control of the rheometer is achieved via a plate that uses the Peltier effect to control the temperature of the sample to within ±0.1 °C. The rheological characterization included measurements of shear viscosity $\mu(\dot{\gamma})$, the first normal-stress difference $N_1(\tau)$, the storage modulus $G'(\omega)$ and the loss modulus $G''(\omega)$.
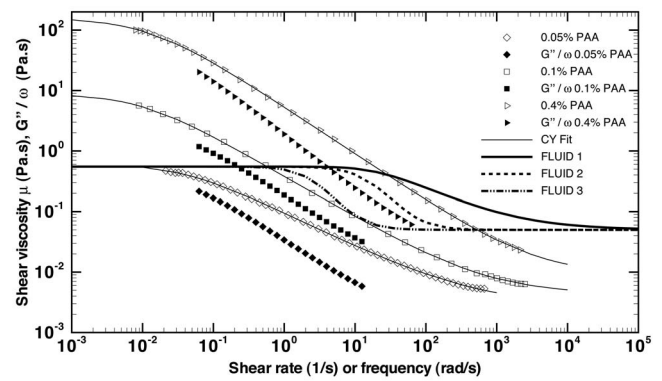

FIG. 2. Shear viscosity and dynamic viscosity (G''/ω) versus shear rate or frequency for polyacrylamide solutions (including Carreau-Yasuda fits and PTT models); hollow symbols represent data obtained in steady shear, and filled symbols represent data obtained in SAOS.

III. WORKING FLUID CHARACTERISTICS

The working fluids used in this investigation were various concentrations (0.05%, 0.1%, and 0.4%) by weight of aqueous solution of a polyacrylamide (PAA), Separan AP273 E supplied by Floerger. The solvent was filtered tap water with 100 ppm of 40% formaldehyde solution added to retard bacterial degradation. Approximately 0.25 g of Timiron seeding particles were added to the working fluid (total volume 575 l) to improve the LDA signal quality. PAA was chosen as it is highly viscoelastic, is optically transparent (thereby permitting LDA measurements) and has been used extensively in previous investigations in our laboratory.[16,17] This polymer is generally regarded[18] as being "very flexible" in its molecular structure and it is this flexibility which gives the liquid more pronounced elastic properties than other water-soluble polymers such as xanthan gum and carboxymethylcellulose. The average molecular weight for the PAA used in this study, ascertained using gel phase chromatography, was determined to be 1.94×10^6 g/mol.

The measured flow curves (shear-viscosity versus shear-rate data) for the three concentrations of PAA are shown in Fig. 2 together with the corresponding Carreau-Yasuda model fits,

$$\mu_{CY} = \mu_\infty + \frac{\mu_0 - \mu_\infty}{(1 + (\lambda_{CY}\dot{\gamma})^a)^{n/a}}, \tag{1}$$

μ_0 being the zero-shear-rate viscosity, μ_∞ is the infinite-shear-rate viscosity, λ_{CY} is a constant which represents the onset of shear thinning, n is a power-law index, and a is a second power-law index introduced by Yasuda et al.[19] The parameters are listed for the various concentrations in Table I and were determined using the least-squares-fitting procedure outlined by Escudier et al.[20]

The measured variation of the first normal-stress difference coefficient Ψ_1 with shear rate is plotted in Fig. 3, which includes data from the PTT models used in the calculations. Although clearly desirable, it is unfortunately not possible to measure the second normal-stress difference with our current instrumentation. For the lower concentration (0.05%) the first normal stress difference N_1 values produced were below

TABLE I. Carreau-Yasuda model parameters for each concentration of polyacrylamide.

c (%)	μ_0 (Pa s)	μ_∞ (Pa s)	λ_{CY} (s)	n	a
0.05	0.614	0.00282	25.7	0.578	0.989
0.1	8.83	0.00437	104	0.679	0.969
0.4	162	0.00937	78.9	0.779	0.888

TABLE II. Power-law parameters for normal-stress variation $N_1 = b\tau^m$ for polyacrylamide.

c (%)	Range of τ (Pa)	b (Pa^{1-m})	m
0.1	2.0–16	19.0	1.07
0.4	20–40	0.114	2.58

the sensitivity of the rheometer even at the highest shear stresses. We also analyzed the variation of N_1, which is a good indicator of the level of elasticity of a fluid, with shear stress τ and found that in the measured range for 0.1% and 0.4% PAA, the recoverable shear $N_1/(2\tau)$ is much greater than 0.5 indicating a highly elastic liquid.[21] A power-law fit to the N_1 (τ) data (i.e., $N_1 = b\tau^m$), not shown in the figure, produces the parameters listed in Table II.

The viscoelastic properties of the PAA solutions were also investigated using small amplitude oscillatory shear (SAOS) measurements and these data are included in Figs. 2 and 3 in terms of the dynamic viscosity, G''/ω, and the dynamic rigidity, $2G'/\omega^2$, plotted against angular frequency, ω. We have used filled symbols to differentiate the SAOS data from the steady shear data. A linearity check was conducted to determine the extent of the linear viscoelastic region prior to the frequency sweep. The frequency sweep data shown in Figs. 2 and 3 was performed at a shear stress of 0.5 Pa, a value well within the linear regime and comparison with data at a higher shear stress, again within the linear regime, confirmed that the viscoelastic properties observed were independent of the shear stress. Since G' has to be zero for an inelastic liquid, it is evident that the oscillatory data reveal a high degree of elasticity for the PAA solution even for the lowest concentration. The SAOS data for each solution were each fitted to a multimode Maxwell model,[22]

$$G' = \sum_{i}^{4} \frac{\eta_i \lambda_i \omega^2}{1 + (\lambda_i \omega)^2}, \quad G'' = \sum_{i}^{4} \frac{\eta_i \omega}{1 + (\lambda_i \omega)^2} \quad (2)$$

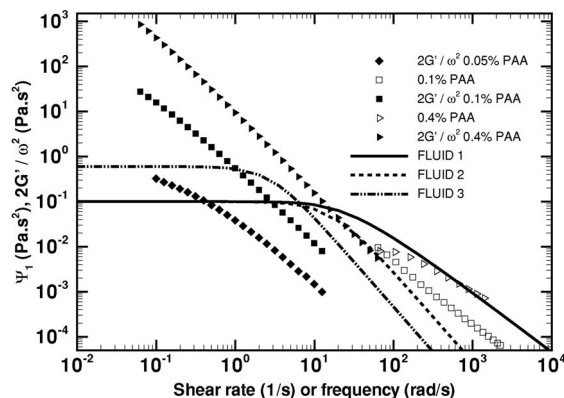which yields relaxation times and viscosity constants which are listed in Table III. In the following section, we shall use these values to estimate an average relaxation time λ for the fluid in order to define a Deborah number for the flow.

IV. ESTIMATION OF REYNOLDS AND DEBORAH NUMBERS

To define Reynolds numbers for the PAA flows, we adopt the bulk velocity at exit from the contraction U_B determined from the volumetric flow rate ($U_B = \dot{Q}_F/wd$) while for the length scale we select the step height ($h = 0.006$ m). The density of the polymer solution was essentially that of the solvent, water. For a shear-thinning liquid no single viscosity can be identified which completely characterizes the fluid and so any definition of a single Reynolds number to characterize the flow is somewhat arbitrary. The surface shear rate at the step inlet has a precise physical interpretation but requires *a priori* detailed knowledge of the flow field to determine its value and cannot easily be used to compare with numerical simulations because, unless the actual and calculated velocity profiles at inlet agree, the Reynolds numbers will differ. In view of this difficulty we favor the use of a more simplistic global Reynolds number Re based upon a viscosity corresponding to a characteristic shear rate defined from bulk-flow quantities, i.e., $\dot{\gamma}_{CH} = U_B/h$. In Table IV, for comparative purposes, we also include a Reynolds number determined using the zero-shear rate viscosity, denoted Re_0.

The Deborah number De is a ratio of two characteristic times, one representing the relaxation processes occurring within a viscoelastic liquid, which we here take as the aver-

FIG. 3. First normal-stress difference coefficient (Ψ_1, hollow symbols) and dynamic rigidity ($2G'/\omega^2$, filled symbols) versus shear rate or frequency for polyacrylamide and PTT models.

TABLE III. Maxwell model parameters for polyacrylamide.

c (%)	λ_i (s)	μ_I (Pa s)
0.05	8.1	0.379
	1.4	0.339
	0.23	0.133
	0.02	0.052
0.1	35.7	1.55
	6.15	0.758
	0.944	0.208
	0.092	0.06
0.4	48.4	82.1
	5.74	10.9
	0.928	2.08
	0.140	0.37
	0.138	0.09

TABLE IV. Fluid and flow parameters for polyacrylamide.

c (%)	U_B (m s^{-1})	$\dot{\gamma}_{CH}=\dfrac{U_B}{h}$ (s^{-1})	μ_{CH} (Pa s)	$Re=\dfrac{\rho U_B h}{\mu_{CH}}$	$Re_0=\dfrac{\rho U_B h}{\mu_0}$	$T_{CH}=\dfrac{h}{U_B}$ (s)	λ_0 (s)	$De_0=\dfrac{\lambda_0}{T_{CH}}$	λ (s)	$De=\dfrac{\lambda}{T_{CH}}$	$E_0=\dfrac{De_0}{Re_0}$	$E=\dfrac{De}{Re}$
0.05	0.260	43.3	0.0134	116	2.5	0.023	2.9	126	$\cdots$	$\cdots$	50	
0.1	0.470	78.3	0.0240	118	0.32	0.013	22.5	1760	0.14	5.8	5500	0.05
0.4	0.128	21.3	0.504	1.5	0.005	0.047	42.2	900	0.11	2.3	189900	1.6
0.4[a]	0.674	112.3	0.145	28	0.025	8.9e$-$3	42.2	4740	0.042	4.7	189900	0.17

[a]Measurements only made within the contraction for this combination of concentration and flow rate.

age relaxation time λ_0 from the multimode Maxwell model fit to the G', G'' data presented in Sec. III and estimated using the expression

$$\lambda_0 = \frac{\Sigma_i^N \lambda_i \eta_i}{\Sigma_i^N \eta_i} \quad (3)$$

and a characteristic time for the flow itself, which we take as h/U_B, i.e., the inverse of the characteristic shear rate. This estimate represents an upper bound of the Deborah number because the λ value determined from oscillatory shear represents the longest relaxation time in the fluid. We denote this parameter De_0. It is also possible to estimate a nonlinear Maxwellian relaxation time from our first normal-stress difference data, where available, using the expression,

$$\lambda = \frac{N_1}{2\tau\dot{\gamma}}. \quad (4)$$

If we use this relaxation time, once again in combination with a characteristic time scale for the flow h/U_B, we can estimate a Deborah number which takes into account the fact that the relaxation time decreases with increasing shear rate. We denote this Deborah number as De. As we could obtain N_1 data only for the two highest concentrations, we cannot estimate a Deborah number in this manner for the 0.05% PAA solution. All of the Deborah and Reynolds number estimates for each flow are listed in Table IV. The large values of De indicate that in all of these flows viscoelastic effects play a major role. Table IV also includes the values of the first elasticity number $E=De/Re$ [based on both zero-shear properties (i.e., $E_0=De_0/Re_0$) and properties determined at a characteristic shear rate (i.e., $E=De/Re$)] to quantify the ratio between the fluid relaxation time and a characteristic diffusion time of the fluid in this geometry.

V. NUMERICAL METHOD

The flow is assumed to be steady, laminar, and incompressible. The governing equations are those expressing conservation of mass,

$$\nabla \cdot u = 0 \quad (5)$$

and momentum,

$$\rho\left[\frac{\partial u}{\partial t} + \nabla \cdot uu\right] = -\nabla p + \eta_s \nabla \cdot \nabla u + \nabla \cdot \tau. \quad (6)$$

The stress field is given by a rheological constitutive equation and here two inelastic models and one viscoelastic model were considered. The purely viscous fluids were modelled as Newtonian and as generalized Newtonian with the viscosity function of the latter given by the Carreau-Yasuda model fit to the experimental rheology data shown in Fig. 2. To represent viscoelastic effects, the PTT model due to Phan-Thien and Tanner[12] was adopted,

$$\lambda\left[\frac{\partial \tau}{\partial t} + \nabla \cdot u\tau\right] + f(\text{tr } \tau)\tau = \eta_p(\nabla u + \nabla u^T)$$
$$+ \lambda(\tau \cdot \nabla u + \nabla u^T \cdot \tau)$$
$$- \xi(\tau \cdot D + D \cdot \tau). \quad (7)$$

The rate of deformation tensor **D** is defined as $D \equiv (\nabla u + \nabla u^T)/2$ and the stress function $f(\text{tr } \tau)$ may follow either the linear form proposed in the original work,[12]

$$f(\text{tr } \tau) = 1 + \frac{\lambda\varepsilon}{\eta_p}\text{tr}(\tau) \quad (8)$$

or the exponential form proposed later by Phan-Thien,[23]

$$f(\text{tr } \tau) = \exp\left[\frac{\lambda\varepsilon}{\eta_p}\text{tr}(\tau)\right]. \quad (9)$$

In Eqs. (6)–(9) the constant model parameters are the relaxation time of the polymer λ, the zero-shear polymer viscosity η_p, the solvent viscosity η_s, the extensibility parameter ε, and the slip parameter ξ. The trace operator (tr) is defined as the sum of the normal stress components of the stress tensor [i.e., $\text{tr}(\tau) = \tau_{xx} + \tau_{yy} + \tau_{zz}$]. A fully implicit finite-volume method was used to solve Eqs. (5)–(7). The method is based on a time marching pressure-correction algorithm formulated with the collocated variable arrangement and is explained in detail in Oliveira $et\ al.$[24] and Alves $et\ al.$[25] Briefly, the governing equations are integrated in space over the control volumes (cells with volume V_p) forming the computational mesh, and in time over a time step (δt), so that sets of linearized algebraic equations are obtained, having the general form,

$$a_P u_P = \sum_{F=1}^{6} a_F u_F + S_U \tag{10}$$

to be solved for the velocity components, and

$$a_p^\tau \tau_P = \sum_{F=1}^{6} a_F^\tau \tau_F + S_\tau \tag{11}$$

to be solved for the extra stress components. In these equations a_F are coefficients accounting for convection and diffusion influences, S are source terms encompassing all contributions not included in the coefficients, the subscript P denotes the cell under consideration and subscript F its corresponding neighboring cells. The central coefficient of the momentum equation a_P is given by

$$a_P = \frac{\rho V_P}{\delta t} + \sum_{F=1}^{6} a_F. \tag{12}$$

Similarly, the central coefficient of the stress equation for the linear PTT model is given by

$$a_p^\tau = \frac{\lambda V_P}{\delta t} + V_P \left(1 + \frac{\lambda \varepsilon}{\eta_P} \mathrm{tr}(\tau_P) \right) + \sum_{F=1}^{6} a_F^\tau \tag{13}$$

and for the exponential PTT model it is sufficient to replace the term in brackets [i.e., the right-hand side of Eq. (8)] by the right-hand side of Eq. (9). Having assembled the coefficients and source terms, the linear sets of Eq. (10) are solved sequentially for the three Cartesian velocity components u, v, and w. These newly computed velocity components do not, in general, satisfy the continuity equation [i.e., Eq. (5)] and need to be corrected by an adjustment of the pressure differences which drive them. This adjustment is accomplished by means of a pressure-correction field obtained from a Poisson pressure equation, derived from the discretized equivalent of Eq. (5) and a simplified form of Eq. (10), which is then solved with a symmetric conjugate gradient method preconditioned with an incomplete LU decomposition. Once a velocity field satisfying continuity has been obtained, the implicitly discretized constitutive equations for the extra stress components [i.e., Eq. (11)] are solved sequentially.

To formulate the convective fluxes, the code uses the high-resolution scheme CUBISTA, formally of second-order accuracy, especially designed for differential constitutive relations.[26] The scheme has the advantage over more classical schemes (e.g., the SMART scheme[27]) of promoting iterative convergence when employed in conjunction with implicit methods.

A. Computational domain and mesh characteristics

The computational domain was chosen to map part of the square inlet duct down to the downstream channel, including the contraction and sudden expansion. The square duct was nearly 5 m long (62 inlet duct hydraulic diameters) and the downstream channel was $120h$ in length in order to ensure fully developed flows upstream and downstream of the contraction and backward-facing steps, respectively. The domain was mapped differently for the inelastic and vis-
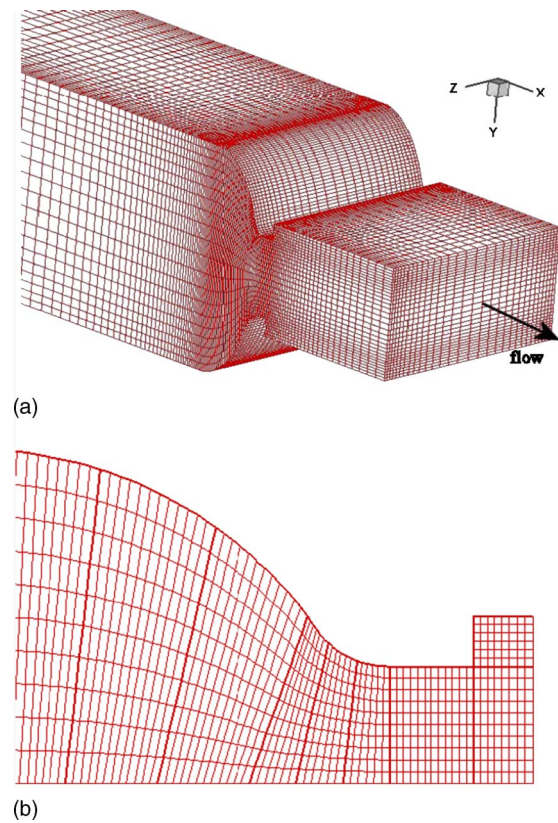

FIG. 4. Mesh used for viscoelastic numerical simulations. (a) 3D view of contraction and expansion region. (b) Detail of mesh in the *XY* symmetry plane.

coelastic computations. For the inelastic calculations, the transverse and spanwise geometric symmetries were used to map a quarter of the geometry with 11 blocks having a total of 27 080 cells (corresponding to 108 320 degrees of freedom), and 10 cells in each the transverse and spanwise directions and a minimum cell size of $(\Delta y)_{\min}/h = 0.108$ and $(\Delta z)_{\min}/h = 0.333$. For the viscoelastic calculations, the domain was mapped from wall to wall, in both the transverse and spanwise directions, with 40 blocks having a total of 102 000 cells corresponding to 1 020 000 degrees of freedom from wall to wall in both the transverse and spanwise directions. For these calculations there were 20 and 30 cells from wall to wall in the y- and z-directions and the minimum cells sizes were $(\Delta y)_{\min}/h = 0.142$ and $(\Delta z)_{\min}/h = 0.397$, respectively. Afonso and Pinho[28] investigated the effect of mesh refinement in this flow problem and showed, in their Figs. 4 and 5, that the use of meshes finer than this one (their M1 mesh) had a weak effect on improving the resolution of the velocity overshoots, at the cost of extremely time-consuming calculations. Very fine meshes are usually required with viscoelastic fluid models when these have unbounded properties, which is not the case for the PTT model, or where very high accuracy is required as in benchmark calculations. The 3D mesh used in the viscoelastic calculations is shown schematically in Fig. 4(a) and a better idea of its characteristics can be gained from the 2D plot across its

TABLE V. Parameters of the PTT models.

	ξ	ε	λ (s)	η_p (Pa s)	η_s (Pa s)	De/Re	De_0/Re_0
Fluid 1	0	0.05	0.1	0.5	0.05	1.343	1.528
Fluid 2	0.2	0.05	0.1	0.5	0.05	1.185	1.528
Fluid 3	0.2	0.005	0.6	0.5	0.05	6.883	9.167

symmetry plane in Fig. 4(b). The calculations were carried out on PC computers with AMD processors at 3.0 GHz and typically took about 72 h to converge.

B. Characteristics of the constitutive equations

Prior to analyzing the results of the numerical calculations, in this section we compare the rheology of the real fluid to the various constitutive models used to perform the flow simulations.

The shear-viscosity behavior of the inelastic model used (Carreau-Yasuda) is an excellent fit to the measured viscosity and is shown in Fig. 2 as solid lines. This figure also includes data pertaining to the various viscoelastic models used in the calculations using the PTT model. A first set of fluids was characterized by a zero second normal-stress difference coefficient ($\xi=0$) and the steady shear rheology partially corresponded to that of the 0.1% and 0.4% PAA solutions. The first set of fluids is well represented by fluid 1 with $\xi=0$, as shown in Fig. 2. Since iterative convergence is difficult whenever $\beta \equiv \eta_s/\eta_0$ is very low or zero, a Newtonian solvent contribution was always used in the calculations with β at least greater than or equal to $1/11$. The incorporation of a Newtonian contribution reduces the width of the power law region of shear viscosity to a narrow range of shear rates between the two Newtonian plateaus. The second set of fluids was identical to the first, except for the second normal-stress difference which was nonzero ($\xi \neq 0$) and is represented in Fig. 2 by fluid 2 with $\xi=0.2$. The values of the parameters for all fluids are listed in Table V including the first elasticity number based on a characteristic shear rate (E) and on zero shear-rate values of the rheological parameters (E_0). Since, as will be seen later, the fluid dynamic predictions with these fluids failed to show key features observed experimentally, these initial calculations were followed by an extensive parametric investigation of the effects of Deborah number, Reynolds number, extensibility, and slip parameters. Some representative results of this third set are shown here, pertaining to fluid 3, which has a shear viscosity close to that of 0.1% PAA within a limited range of shear rates. Although in the parametric study we did not attempt to reproduce the measured rheology of PAA solutions, it turned out that some fluids, such as fluid 3, had a rheology close to that of the real fluids. It would be desirable to perform numerical simulations with fluids having a rheology closer to that of the PAA fluids or with a fluid-like fluid 3 with $\xi=0$, but unfortunately none of these cases converge, i.e., our analysis is limited to cases for which converged solutions can be obtained.

The first normal-stress difference coefficients for the various PTT fluids are compared in Fig. 3 with the measured data. For fluids 1 and 2, the model data are not too different from the measured Ψ_1 values whereas for fluid 3 the model values are at least one order of magnitude lower than those measured. Finally, in Fig. 5, a comparison is made between the Ψ_2 values for fluids 2 and 3 ($\Psi_2=0$ for fluid 1). Although fluid 3 has a higher zero-shear Ψ_2 value than fluid 2, parameters other than ξ also affect the behavior of Ψ_2 and so there is a crossover of this property between fluids 2 and 3.
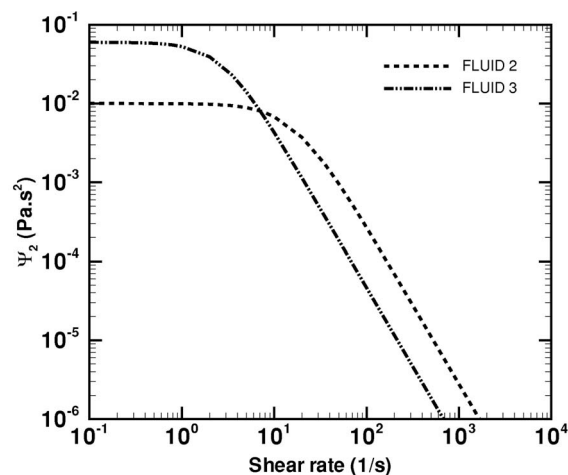
VI. DISCUSSION

To avoid confusion and overcrowding of data within the figures, we present and discuss our experimental results and the viscoelastic simulations separately although the purely viscous (i.e. Newtonian and Carreau-Yasuda model) simulations are included with the experimental results as a basis for comparison.

A. Approach-flow within the square duct

1. Experiments

The flow field within the square duct was mapped out three hydraulic diameters upstream of the gradual contraction/sudden expansion (i.e., at a location $>120 D_H$ downstream of inlet to the square duct). The results are presented in Figs. 6(a) and 6(b). In this and all subsequent figures, filled symbols represent data points reflected about appropriate centerplanes. For the 0.05% concentration of PAA, the velocity profiles shown in Fig. 6(a) (in this figure all velocities are normalized by the bulk velocity within the square duct i.e., $U_{SD}=\dot{Q}_F/w^2$) are power-law-like in appearance, entirely consistent with what is expected for fully de-

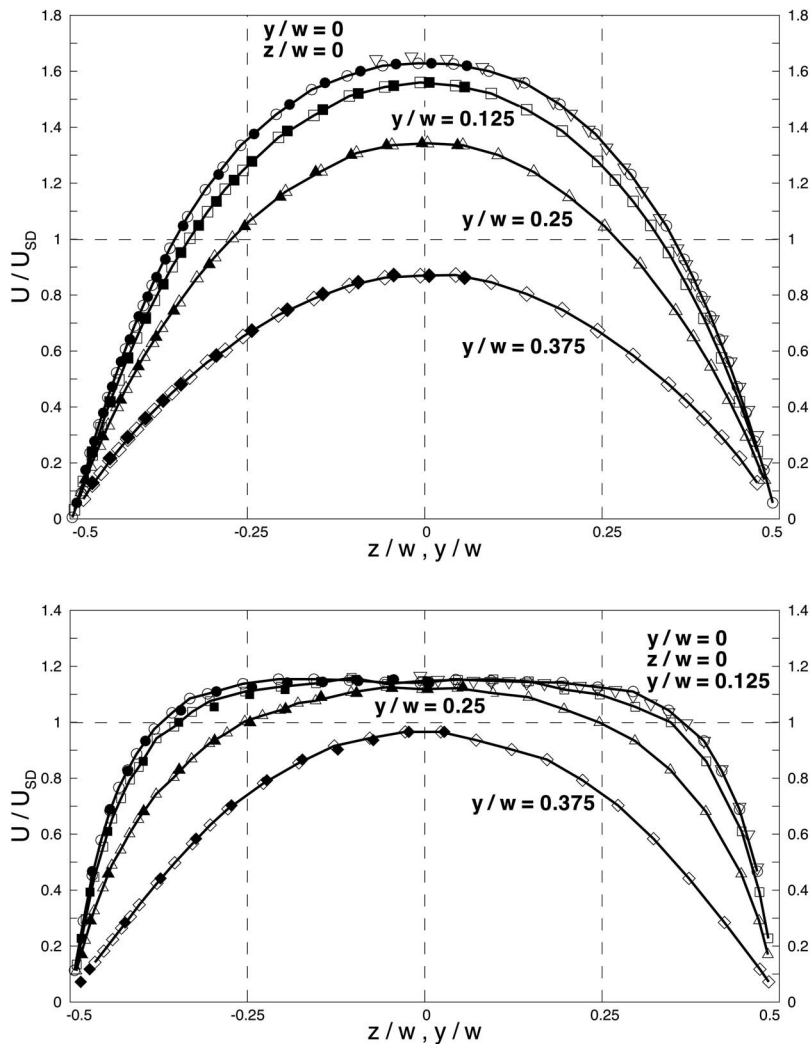FIG. 5. Second normal stress difference coefficient (Ψ_2) for PTT models.

FIG. 6. Streamwise velocity profiles (U/U_{SD}) within the square duct for (a) 0.05% PAA Re=116 and (b) 0.4% PAA Re=1.5. Spanwise variation for y/w=0 (○), 0.125 (□), 0.25 (△), and 0.375 (◇) and transverse variation for z/w=0 (*XY*-centerplane) (▽). (In this and all subsequent figures, symbols represent experimental data and filled symbols represent data points reflected about the appropriate centerplane.)

veloped laminar flow of a shear-thinning, viscoelastic liquid[22,29] and symmetric about both the *XY* and *XZ*-centerplanes. For the highest concentration, 0.4% PAA, shown in Fig. 6(b), the highly shear-thinning nature of this liquid produces velocity profiles which are much flatter in appearance but again symmetric about both *XY* and *XZ*-centerplanes. We also note that the velocity profiles obtained from the Carreau-Yasuda simulation within the square duct [essentially the profiles at $x/h=-7$ shown in Fig. 9(c) below], although flatter than the equivalent Newtonian profiles as might be expected from purely shear-thinning considerations, do not completely match the experimental results. A possible explanation for this difference is that, even at a relatively low polymer concentration (0.05%), this fluid produces second normal-stress differences of sufficient magnitude to induce secondary motion within the square duct which in turn alter the streamwise velocity structure. This secondary motion in fully developed laminar flow of a viscoelastic fluid through a square duct was first investigated numerically by Wheeler and Wissler.[29] More recent papers[30,31] have shown that the magnitude of the secondary-flow velocities are typically two orders of magnitude lower than that of the streamwise velocity. In the current experi-

ments, we estimate that the maximum secondary flow velocities would be of order 10 μm/s, well below the resolution of our LDA system.

2. Viscoelastic simulations

From the outset, for the viscoelastic simulations, it is important to distinguish between the results for models with, and without, a second normal-stress difference. The fully developed flow through a square duct of fluids having a nonzero second normal-stress difference ($\xi \neq 0$) is characterized by a secondary flow in the cross-section which is superimposed on the streamwise flow. This secondary flow arises as a consequence of an imbalance of normal stresses in the cross-section plane and is akin to events for turbulent flow of Newtonian fluids in noncircular ducts,[15,32] although for turbulent flows the sense of the secondary motion is opposite to that for the laminar flow of viscoelastic fluids. This secondary flow does not exist for laminar flows of models with zero second normal-stress difference in steady shear, such as the simplified PTT ($\xi=0$), Newtonian and generalized Newtonian constitutive equations. As will be seen in the numerical results later, small cat's ears were only observed here in the
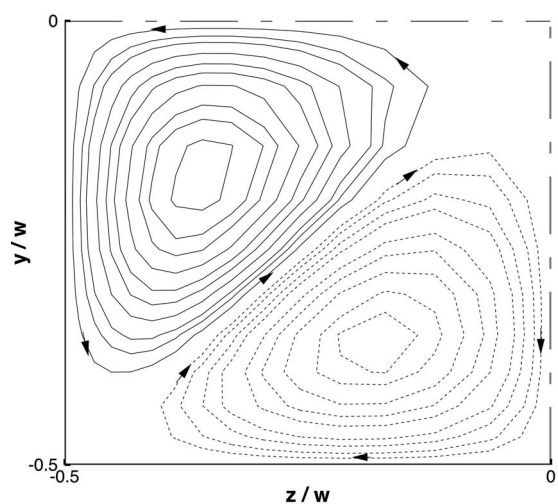
FIG. 7. Simulated secondary-flow cross-stream streamlines under fully developed conditions in a quadrant of the square duct at $x/h = -70$ for fluid 2 ($\xi = 0.2$, De$=7.85$, Re$=6.62$, and Re$_0 = 5.14$). Short dashed lines (- - -) correspond to negative values of the stream function, sense of direction indicated by arrowheads, and centerplanes shown by long dashed lines (– - –).

presence of secondary flows, in combination with strong strain hardening (low values of ε), high Deborah numbers and some inertia. Unfortunately, for low values of ε and high values of De, the simulations do not converge when setting ξ to very low values ($\xi < 0.1$) and zero, due to the high Deborah number problem (the growth of large normal stresses and stress gradients associated with the distortion term of the Oldroyd derivative). Converged solutions with $\xi = 0$ were only achieved with high values of ε and or low values of De, in which case no cat's ears were observed (maps of converged solutions as a function of rheological parameters are presented in Afonso and Pinho[28]). As a consequence it was not possible to demonstrate unequivocally whether $\xi \neq 0$ is essential to obtain cat's ears. As we will discuss later there are indications from a related geometry that cat's ears can be predicted with $\xi = 0$ provided ε is very small and De is large.

The strength of the secondary flow depends on the values of both ξ and the relaxation time λ and in Fig. 7 we show the cross-stream streamlines for fluid 2. Streamlines are only shown for this simulation because, much as was observed by Xue et al.,[33] the *pattern* of the secondary flow is essentially unaltered by the PTT model parameters. Symmetry has been assumed about the horizontal and vertical planes but not about the diagonals. Although there are slight differences between the two sectors of the quadrant shown in Fig. 7, primarily as a consequence of the extremely small values of the secondary flow velocities, the flow is essentially symmetric in both cross-stream directions. The spanwise and transverse profiles coincide as they should for fully developed flow confirming the essential symmetry of the flow. We utilize this symmetry to plot in a compact manner several streamwise velocity profiles in Fig. 8. As in the experiments, the maximum streamwise flow velocities are about 0.32 m/s while the secondary flow velocities are close to 0.0002 m/s i.e. three orders of magnitude lower. Similar results were obtained by Gervang and Larsen[30] and Debbaut et al.[31] although the latter found that "both velocity components in the cross-section plane are typically two orders of magnitude lower than the axial velocity." When the value of ξ decreases, the secondary flow weakens and so the maximum secondary-flow velocities decrease while the maximum streamwise velocity remains essentially the same. Since the secondary flow is much weaker than the streamwise flow (at most less than 0.1% of the streamwise velocity), the shear viscosity is basically determined by the streamwise flow. There is also an effect of ξ in lowering the shear rate at which shear thinning begins and also narrowing the range of shear rates over which shear thinning occurs, as shown in Fig. 2. However there is no change in the shape of the inlet streamwise flow between fluid 1 with $\xi = 0$ and fluid 2 with $\xi = 0.2$ (these data are not shown here for conciseness). In going from fluid 1 (left-hand side of Fig. 8) to fluid 3, also with $\xi = 0.2$ (right-hand side of Fig. 8), the velocity profiles flatten because the variable shear viscosity region moves to
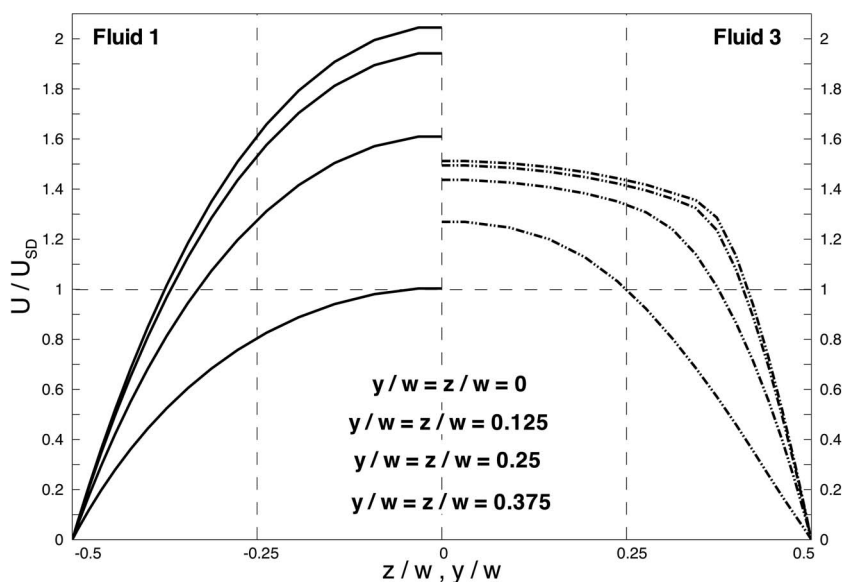

FIG. 8. Simulation of velocity profiles within square duct. LHS: Fluid 1 ($\xi = 0$, De$=7.85$, Re$=5.84$, and Re$_0 = 5.14$); RHS: Fluid 3 ($\xi = 0.2$, De$=39.23$, Re$=5.70$, and Re$_0 = 4.28$).
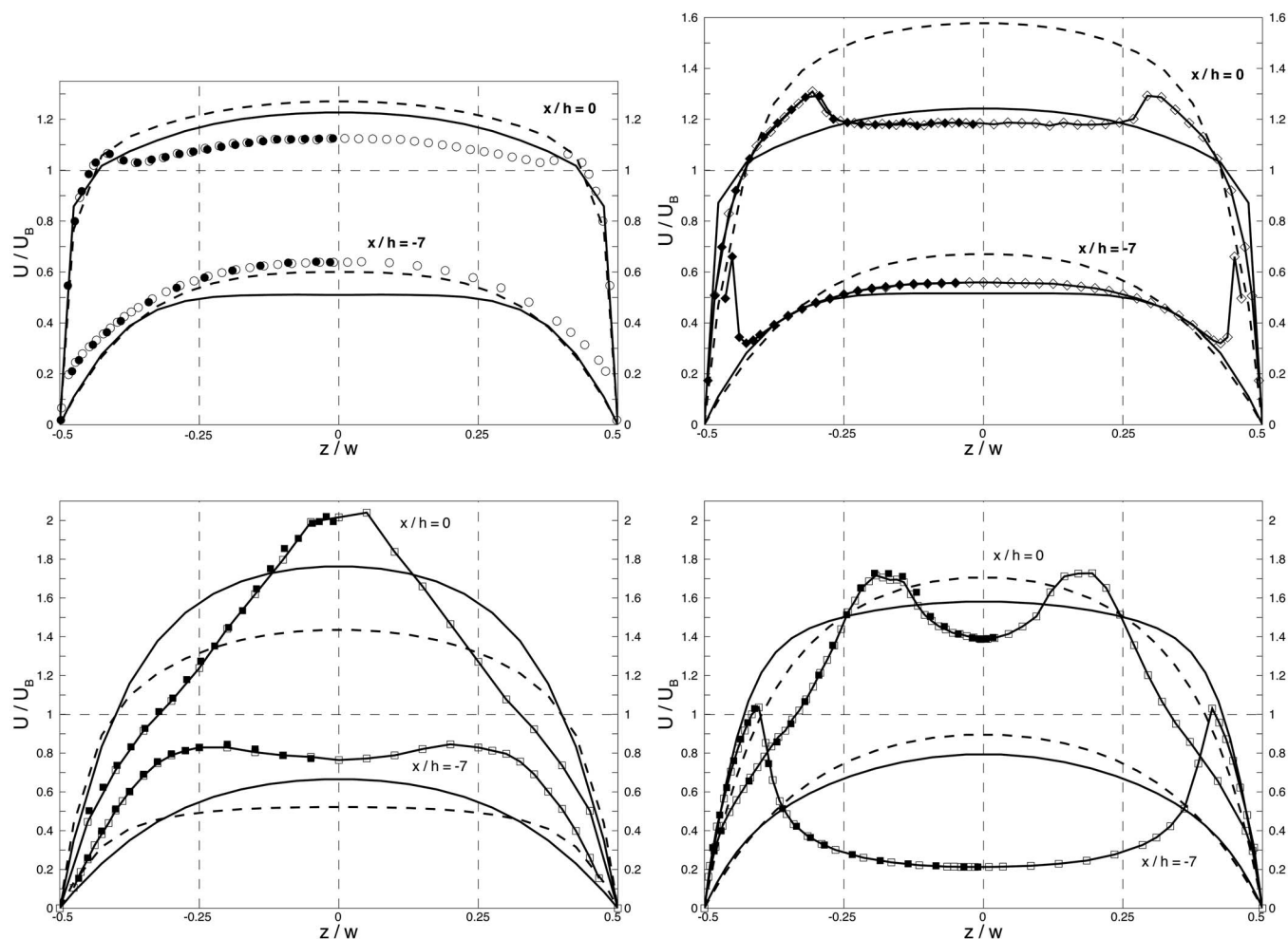
FIG. 9. Velocity profiles for $y/D=0$ (XZ centerplane) within contraction. Simulations for Newtonian fluid (solid line) and generalized Newtonian fluid (dashed line): (a) 0.05% PAA Re=116, (b) 0.1% PAA Re=118, (c) 0.4% PAA Re=1.5, and (d) 0.4% PAA Re=28.

even lower shear rates because of the higher value of λ. Therefore, it is not completely unexpected that the differences in inlet velocity profile between the left and right-hand sides of Fig. 8 are qualitatively similar to the changes observed between the inlet velocities of 0.05% PAA in Fig. 6(a) and 0.4% PAA in Fig. 6(b).

B. Flow field within the gradual contraction

1. Experiments

Distributions of streamwise velocity within the XZ-centerplane, both just within the gradual contraction (at $x/h=-7$) and at the contraction exit (i.e., just before the backward-facing step, $x/h=0$) are shown in Figs. 9(a)–9(d). For 0.05% PAA, the lowest concentration, shown in Fig. 9(a), the velocity profile at the start of the contraction ($x/h=-7$) is hardly changed from the approach flow in the square duct, i.e., the profile is essentially power-law-like in appearance. At $x/h=0$, away from the side walls, the flow is again unremarkable; the velocity in the central region of the flow (i.e., $-0.25<z/w<0.25$) has increased in magnitude compared to the profile at $x/h=-7$ as a consequence of the reduction in duct cross-sectional area. Outside of this central

region, located at approximately $z/w=\pm0.4$, small velocity overshoots are apparent. Although smaller in magnitude than those observed by Poole *et al.*,[6] these overshoots are similar in appearance to their cat's ears profiles and must be a manifestation of the same phenomenon. As the PAA concentration and solution rheology are the same as in Poole *et al.*,[6] and the Reynolds number approximately the same, the reduction in magnitude of the overshoots in the current study is attributed to the smaller area contraction ratio (2.86:1 compared to 8:1).

When the PAA concentration is increased to 0.1%, Fig. 9(b), the cat's ears are significantly enhanced and present at both $x/h=-7$ and $x/h=0$. Although increasing the PAA concentration leads to an increase in both the degree of shear thinning (see Fig. 2) and the level of elasticity (see Fig. 3 and Table III), as we have matched the Reynolds number for the two flows ($\sim$120), it is possible to identify some criteria under which velocity profiles with the cat's-ears form are likely to occur. As can be observed in Figs. 9(a) and 9(b), by comparison of the Newtonian and GNF simulations, the effect of shear thinning, in the absence of elastic effects, is clearly not responsible for the cat's ears. The major differ-

ence between the 0.05% PAA and 0.1% PAA flows is the increased viscoelasticity of the liquid for the higher concentration. This increase is reflected in the respective Deborah and elasticity numbers number for the two flows: De_0 and E_0 for the 0.1% PAA flow are more than an order of magnitude greater than the values for the 0.05% PAA flow ($De_0 = 1760$ compared to 126 and $E_0 = 5500$ compared with 50).

With further increases in PAA concentration, to 0.4%, the LDA measurements showed that at a Reynolds number of about 120 (i.e., the same as for the 0.05% and 0.1% PAA flows) the flow field within the contraction became unsteady. This unsteadiness is probably an elastic instability due to the extremely high Deborah number (in excess of 10 000) of this flow. Results for the 0.4% solution are presented for two lower Reynolds numbers: 1.5, where the flow remained steady both within the contraction and also downstream of the step, and 28, where the flow was steady within the contraction but showed signs of unsteadiness downstream of the step. These unsteady results are not reported in detail here, and results downstream of the step are reported only for Re=1.5 (see Fig. 15 below). For the flow within the contraction at this low Re, Fig. 9(c), despite not exhibiting the cat's ears the profiles are nevertheless quite remarkable. Just within the contraction, at $x/h = -7$, there are marginal velocity "overshoots" located much nearer the centerline (at $z/w = \pm 0.25$) than for the lower concentrations. By the contraction exit, $x/h = 0$, the central core region of the flow has accelerated significantly resulting in a profile almost triangular in shape. Increasing the flow rate for this high-concentration fluid, Fig. 9(d), has the effect of increasing both De and Re; once again a cat's ears profile, albeit in a somewhat different form, is evident. For this flow the velocity overshoots near the sidewalls for the $x/h = -7$ profile are at their most exaggerated; the peak velocity is nearly five times that for the flow in the center of the duct. From the experimental results it may be concluded that the cat's ears are most likely to appear for flows with relatively high levels of both inertia (i.e., Re > 10) and elasticity.

2. Viscoelastic simulations

For fluids 1, 2, and 3, Fig. 10 shows the progression of the streamwise velocity within the contraction along the XZ centerplane, where we see some small velocity overshoots appearing. Along the XY centerplane the cat's ears effect is considerably less pronounced than in the XZ centerplane, as seen in the comparison between Figs. 11(a) and 12 and in the extensive comparisons of Afonso and Pinho;[28] hence our analysis is essentially on the latter plane.

The simulations of flows of fluid 1, at Reynolds numbers around 5–10, as was also the case for the experiments with 0.4% PAA, do not show any remarkable feature, such as cat's ears, in spite of shear-thinning and viscoelastic rheological characteristics (N_1). Increasing the viscoelasticity while maintaining $\xi = 0$ eventually leads to divergence of the code before any hint of a velocity overshoot appears, as seen in Afonso and Pinho.[28] Introducing nonzero second normal stress differences ($\xi \neq 0$ but not too high) allows converged solutions in many cases for which the corresponding $\xi = 0$
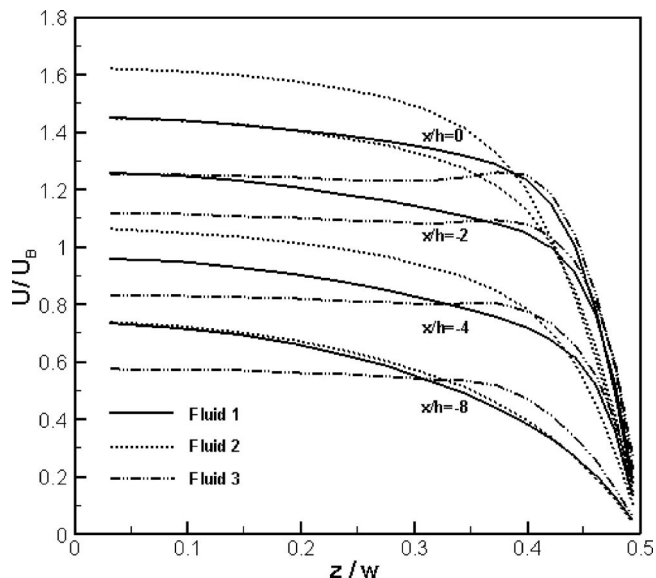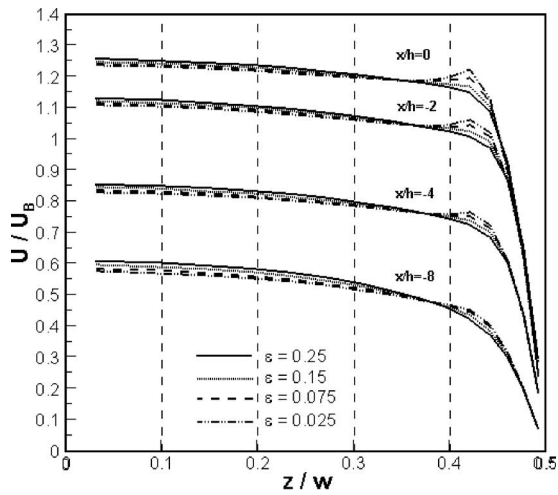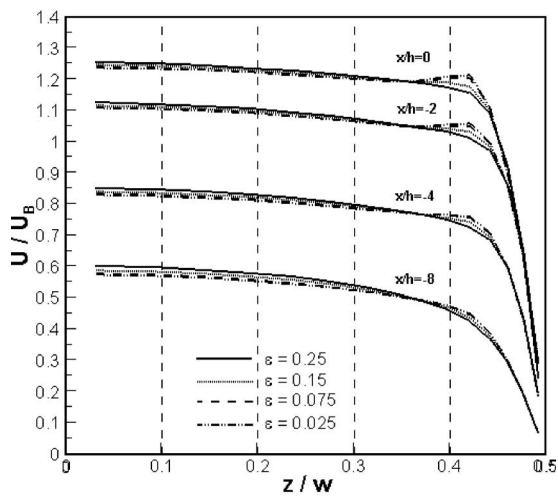

FIG. 10. Simulated velocity profiles within contraction for various viscoelastic simulations in the XZ centerplane: Fluid 1 ($\xi = 0$, De=7.85, Re=5.84, and $Re_0 = 5.14$), fluid 2 ($\xi = 0.2$, De=7.85, Re=6.62, and $Re_0 = 5.14$), and fluid 3 ($\xi = 0.2$, De=39.23, Re=5.70, and $Re_0 = 4.28$).

case would diverge. For the set of converged solutions we obtained an increase in the viscoelasticity for fluids with nonzero second normal-stress differences, such as fluid 3 in Fig. 10, which has a lower value of ε and the same high value of ξ as fluid 2, leads to the appearance of a small velocity overshoot located at approximately the same location as it was seen in the experiments, i.e., $z/W \approx 0.4$. Simultaneously with the overshoot in the XZ centerplane, an overshoot is also formed in the XY centerplane as seen in Fig. 12, but only within the contraction. The absence of overshoot at the exit of the contraction in this symmetry plane could be a consequence of the well-known smoothing effect of contractions. These effects on both symmetry planes were never observed in the calculations for fluids without N_2 in this geometry bearing in mind that the use of very small values of ε, such as $\varepsilon = 0.005$, in combination with $\xi = 0$, does not lead to a converged solution. If such simulations were to converge it is not unlikely that velocity peaks could appear for low ε and high De with $\xi = 0$. Even with nonzero N_2, cat's ears are not observed if $\xi < 0.2$ or if ε is large with $\xi = 0.2$ as in Fig. 11.
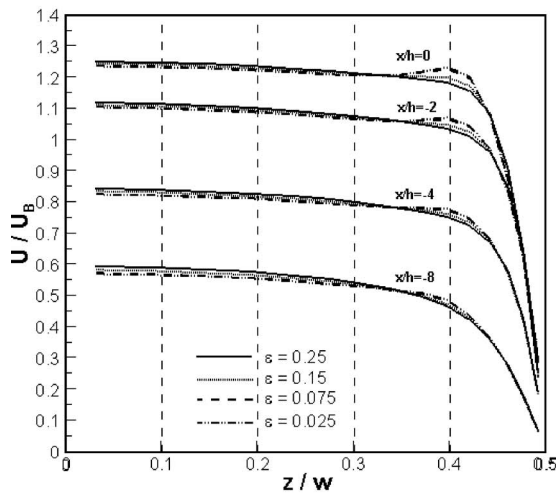
In their parametric investigation, Afonso and Pinho[28] performed more than 100 calculations to separately assess the effects of De, Re, as well as of ε and ξ of the PTT model. When observed, the cat's ears on the XZ centerplane were of this order of magnitude, although in some cases it could be more intense, but never attaining the same level as observed in the experiments. In Figs. 11 and 12 we show some of those results, in particular the effects of Deborah number and ε on the velocity profiles in the XZ and XY symmetry planes, respectively. These calculations correspond to the same zero shear rate Reynolds number Re_0 of 5.14 and $\xi = 0.2$ for which the cat's ears were more pronounced. The figures show that increasing strain-hardening for the extensional viscosity, i.e., lowering ε, reduces the velocity on the center of the duct

(a)

(b)

(c)

FIG. 11. Effect of ε on development of velocity profiles within contraction for $y/w=0$ (*XZ* centerplane) for various PTT fluids at $Re_0=5.14$ and with $\xi=0.2$: (a) De=19.6, (b) De=23.5, (c) De=31.4.

thus enhancing the wall peak, while increasing the Deborah number has two effects: broadening the cat's ears and moving them towards the center of the duct without changing significantly the value of the peak velocity. Unfortunately,
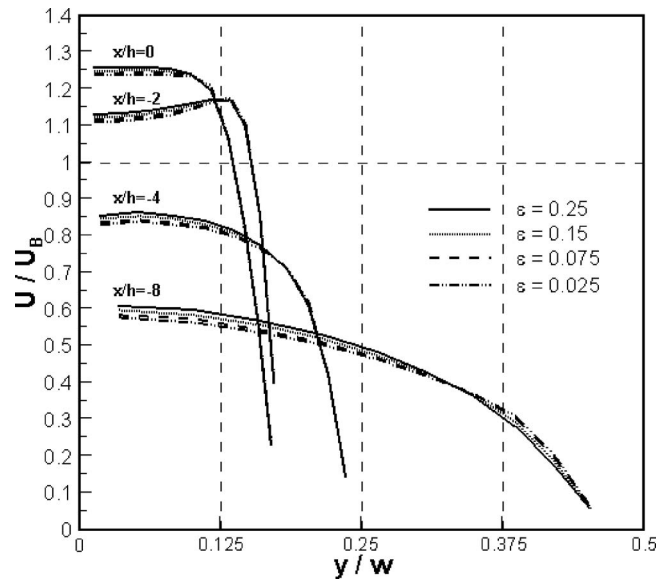

FIG. 12. Effect of ε on development of velocity profiles within the contraction for $z/w=0$ (*XY* centerplane) for various PTT fluids at $Re_0=5.14$, De =19.6 and with $\xi=0.2$.

converged solutions could neither be attained with higher values of ξ, nor with $\xi=0$ using very small values of ε ($\varepsilon \leq 0.005$) as explained in more detail by Afonso and Pinho.[28] To clarify the effect of ξ, in Fig. 13 we show velocity profiles in the *XZ* centerplane for a different high De case with a value of ε that allows converged solutions to be obtained. We see clearly that ξ facilitates the appearance of cat's ears close to the wall.

More details of the extensive calculations just outlined are presented in Afonso and Pinho[28] where we conclude that for cat's ears to be observed with the PTT model, in this
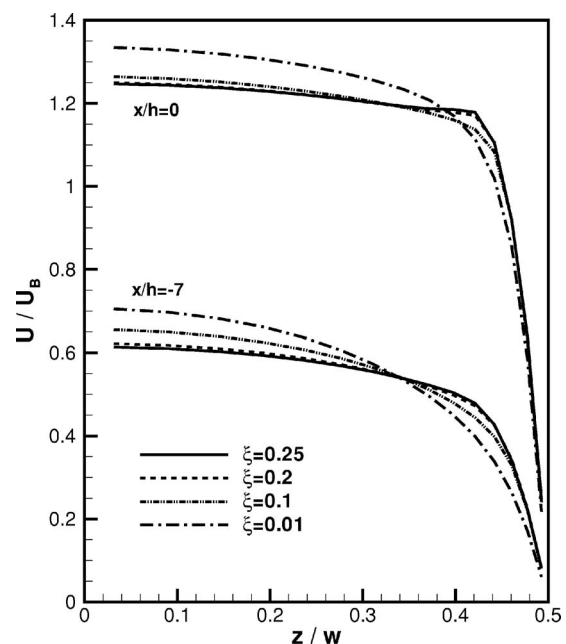

FIG. 13. Effect of ξ on development of velocity profiles within the contraction for $z/w=0$ (*XY* centerplane) for various PTT fluids at $Re_0=5.14$, De =19.6 and with $\varepsilon=0.15$.
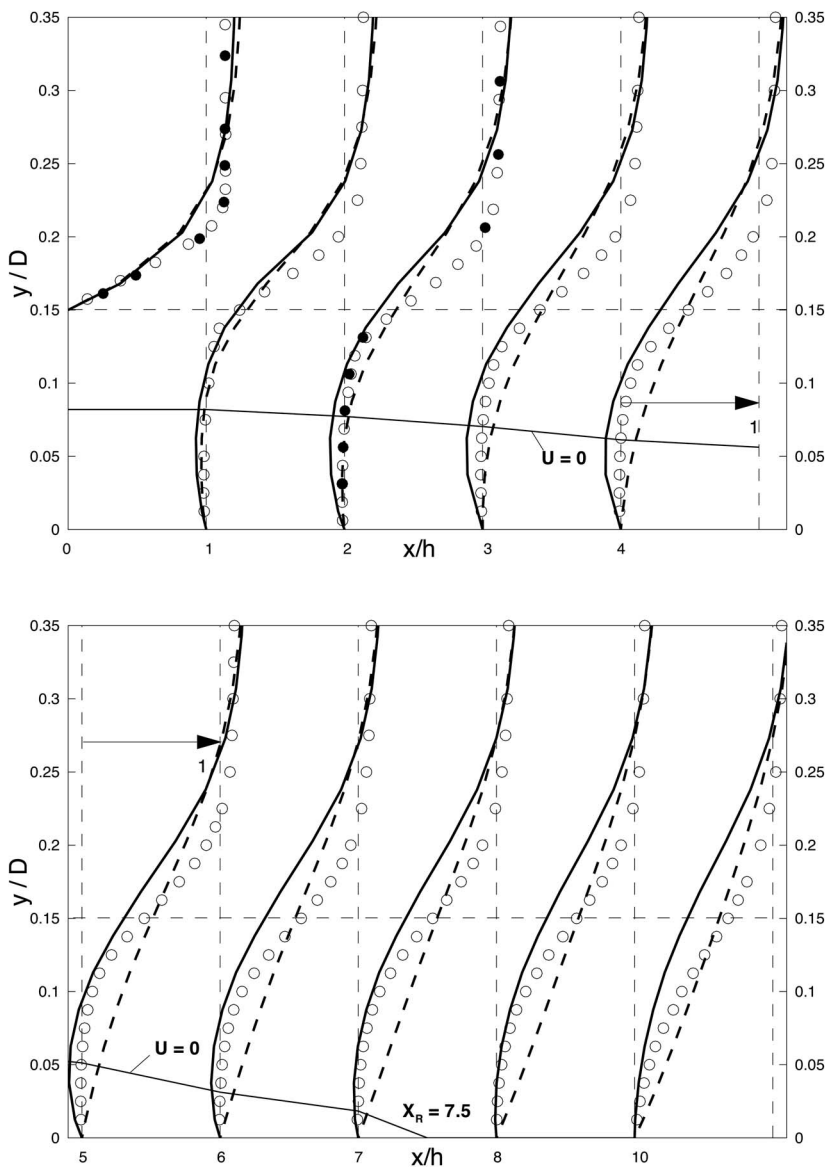
FIG. 14. Velocity profiles for $z/w=0$ (XY centerplane) downstream of expansion for 0.05% PAA at Re=116. Newtonian simulation (solid line) and GNF simulation (dashed line): (a) $0<x/h<4$; (b) $5<x/h<10$.

particular geometry and based on the converged set of solutions, a very high second normal-stress difference is required (high values of ξ) in combination with high extensional viscosities (low values of ε), some inertia and high Deborah numbers. This does not mean that a nonzero ξ is an absolute requirement to observe velocity overshoots in smooth contractions, but is needed in this particular case where the contraction ratio is not very high (8:2.86) and there is also a sudden expansion that does not allow converged solutions to be obtained for small values of ε (Poole *et al.*[34]). In fact, Alves[35] has recently observed small cat's ears in a 4:1 smooth contraction without a sudden expansion using a model that predicts a vanishing N_2 in steady shear (essentially three-dimensional calculations of the geometry used in Alves and Poole[36]). His observation suggests that the phenomenon could be observed with other Maxwell-type models and to be independent of whether the fluid has N_2, provided one is able to obtain converged solutions. It is probable that

in our geometry the secondary flow, which is a consequence of N_2, reduces the high stresses and high stress gradients responsible for the divergence of the code, while not eliminating velocity overshoots and so we are able to obtain converged solutions for low values of ε and high De, which would otherwise be impossible to achieve with $\xi=0$. At low and high inertia, maintaining the other parameters unchanged, the cat's ears disappear, but at low inertia the velocity profiles at the exit of the contraction become narrow. The results emphasize the very rich dynamics of complex flows of viscoelastic fluids under conditions of nonnegligible inertia.

C. Flow field downstream of the step

1. Experiments

The flow field downstream of the step is represented by the transverse variation of streamwise velocity profiles in the
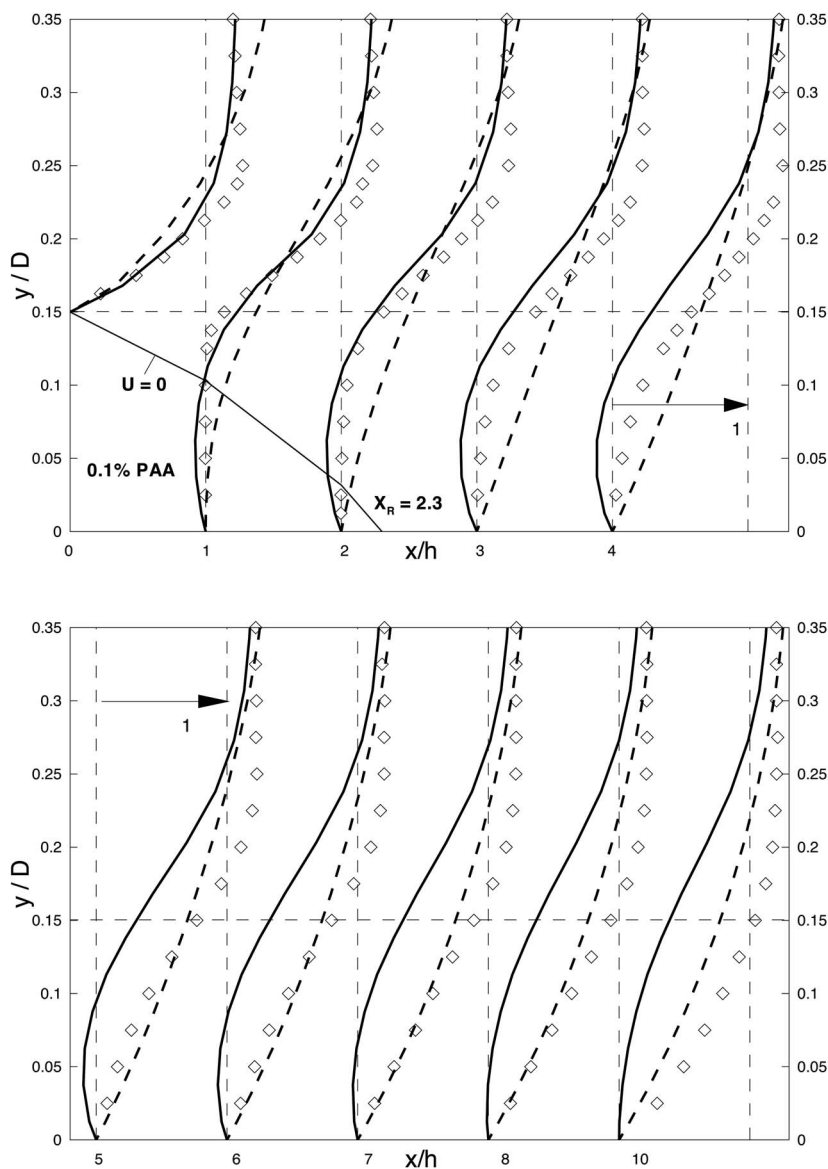
FIG. 15. Velocity profiles for $z/w=0$ (XY centerplane) downstream of expansion for 0.1% PAA at Re=118. Newtonian simulation (solid line) and GNF simulation (dashed line): (a) 0 $<x/h<4$; (b) 5$<x/h<10$.

XY-centerplane for PAA concentrations of 0.05%, 0.1%, and 0.4% which we present in Figs. 14(a), 14(b), 15(a), 15(b), 16(a), and 16(b), respectively.

As can be seen in Fig. 14, for the lowest PAA concentration, the non-Newtonian effects on the streamwise velocity profiles, in the XY-centerplane at least, appear to be modest. There is little effect on the length of the recirculation region although the magnitude of recirculating velocities is diminished compared to that for the flow of a Newtonian fluid. Differences in the flow structure between the polymer solution and the inelastic simulations are probably related to differences in the velocity profiles at the inlet which, in turn, are a consequence of the gradual contraction.

Increasing the concentration to 0.1% PAA leads to a significant reduction in both the intensity and the length of the recirculation region. This attenuation, seen in Fig. 15, is perhaps unsurprising given that recirculation is known to be reduced by high levels of both shear thinning, through the

redistribution of inertia,[37] and viscoelasticity, by normal-stress effects.[9] At the highest PAA concentration (0.4%) we present results at a Reynolds number of 1.5 (Fig. 16) because, as we have already indicated, steady flow could not be realized at the same high Reynolds number as for the lower concentration PAA flows. The most striking feature of the results presented in Fig. 16 is the shape of the velocity profile at inlet (i.e., $x/h=0$): much as was observed for the inlet profile in the XY-centerplane [Fig. 9(c)] the profile is almost triangular in form but in addition now exhibits inflections. Points of inflection are necessary conditions for inviscid instability (Rayleigh criterion), and increase the region where infinitesimal disturbances are amplified and the flow becomes unstable (i.e., the neutral curve is widened and no longer closed).[38] Their existence then may well explain the loss of steadiness which we observe experimentally for the flow of this high concentration at Re$\sim$100.
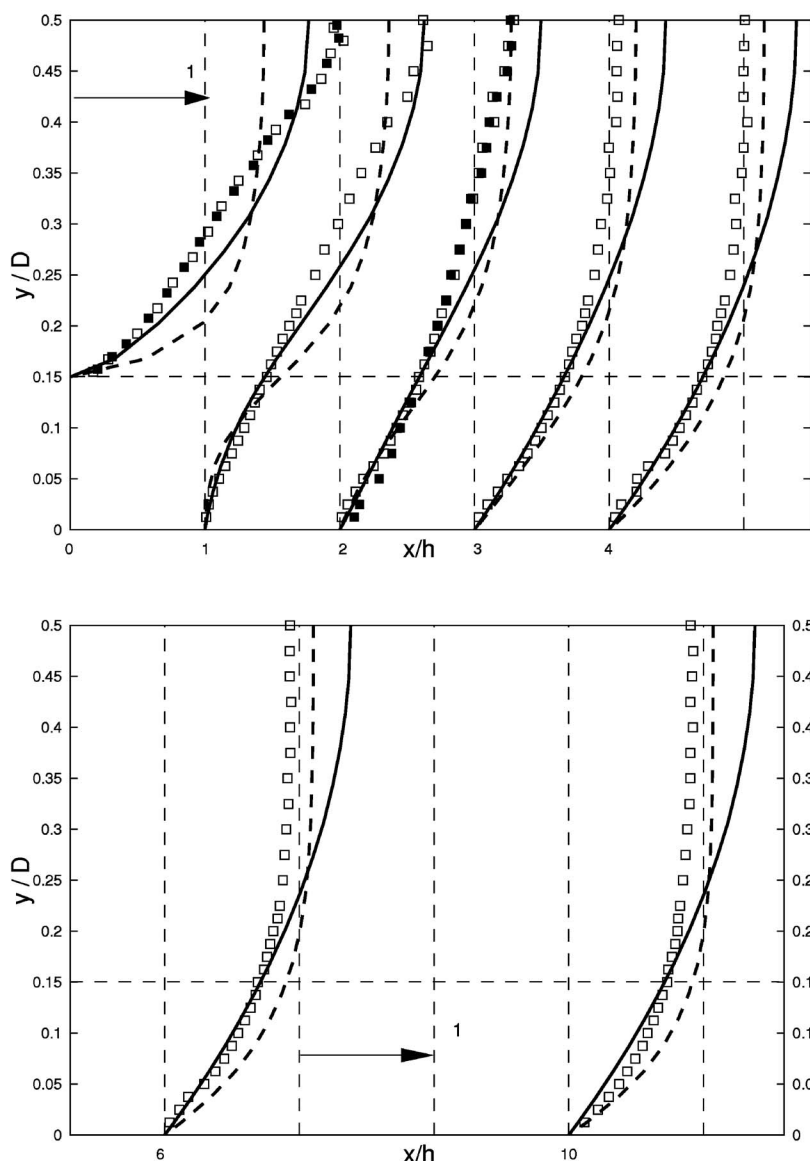
FIG. 16. Velocity profiles for $z/w=0$ (XY centerplane) downstream of expansion for 0.4% PAA Re=1.5. Newtonian simulation (solid line) and GNF simulation (dashed line). (a) $0<x/h<4$; (b) $5<x/h<10$.

2. Viscoelastic simulations

The transverse variation of the mean streamwise velocity profiles in the XY centerplane downstream of the expansion is plotted in Fig. 17 for PTT fluids 1, 2, and 3 and compared with the experimental data for 0.4% PAA. Downstream of the expansion the results of the simulations of fluids 1 and 2 are similar, whereas fluid 3 underpredicts the centerline and the wall regions. The simulation of fluid 2 predicts the flow between the wall and y/D of around 0.2 fairly well, showing also no recirculation at the plotted stations. The results of fluid 1 and fluid 2 are broadly similar except that fluid 1 underpredicts fluid 2 between the wall and y/D of around 0.3 and overpredicts nearer the center. Fluid 3 is in poorer agreement with the experimental data. Nevertheless, the viscoelastic predictions are an improvement over the predictions by both the GNF and the Newtonian simulations shown in Fig. 16. The central jet, however, is underpredicted at the inlet of the expansion and the rapid reduction of the jet with downstream distance is also not well captured since, for $x/h>2$, the predictions always exceed the measured data in the cen-

tral region of the duct. A similar result had already been obtained by Poole *et al.*[39] for a PTT fluid akin to fluid 1 with $\xi=0$ and a shear viscosity closely matching the viscosity of the 0.4% PAA. Here, the results for fluids with nonzero second normal stress differences, which allowed prediction of small cat's ears, are still not able to capture completely the triangular shape of the streamwise velocity profile at the inlet to the sudden expansion.

VII. CONCLUSIONS

The results have been reported of an experimental and numerical investigation of the laminar flow of a series of viscoelastic liquids (concentrations of a polyacrylamide in the range 0.05%–0.4%) over a symmetrical, double backward-facing step geometry of expansion ration 1.43. The expansion duct is preceded by a gradual contraction, with an outlet of aspect ratio 2.86:1, upstream of which is a long (120 hydraulic diameters) square duct.

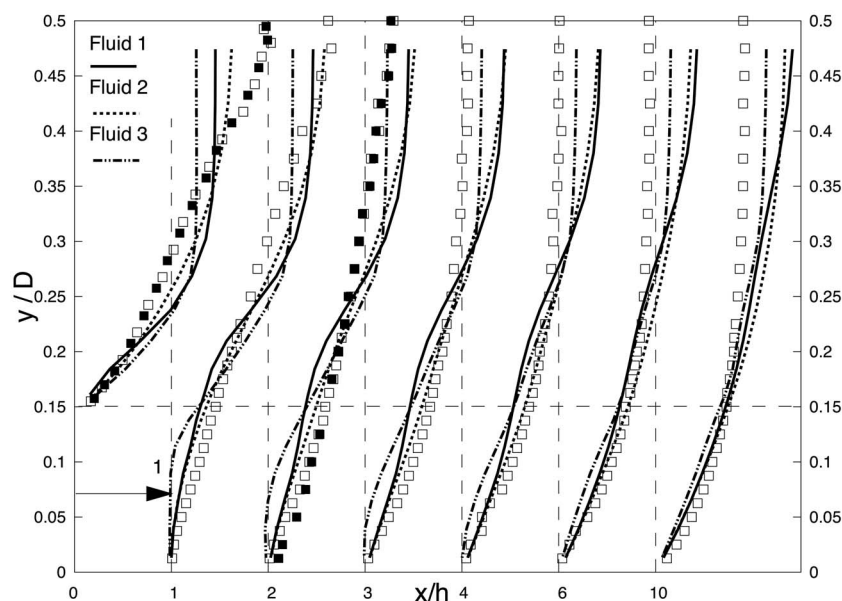The fully developed flow in the square duct upstream of

FIG. 17. Transverse variation of mean streamwise (U/U_B) velocity profiles in the *XY*-centerplane (i.e., $z/w=0.5$) downstream of expansion for the viscoelastic simulations with the PTT model (continuous lines). Experimental results for 0.4% PAA at Re=1.5 (open symbols). Fluid 1 ($\xi=0$), Re =5.8, Re_0=5.14, fluid 2 ($\xi=0.2$), Re =5.6, Re_0=5.14 and fluid 3 Re=5.7, Re_0=5.14.

the gradual contraction is unremarkable but flow through the contraction that precedes the expansion is fundamentally different from the equivalent Newtonian fluid flow. As the flow progresses through the contraction, velocity overshoots develop adjacent to the flat sidewalls of the contraction that, due to their appearance, in a recent related paper we have dubbed cat's ears. There is an abrupt change from the nearly two-dimensional flow in the central region of the contraction with extremely high velocity gradients evident in the velocity overshoots. The exact shape and magnitude of the cat's ears are found to be Reynolds number and Deborah number dependent.

Downstream of the step the effects of viscoelasticity are less significant and any discrepancies between the experiments and simulations are related to differences in the inlet velocity profile which, in itself, is a consequence of the gradual contraction. As the polymer concentration is increased, the combined effects of increased shear thinning and viscoelasticity are found to reduce dramatically the length and magnitude of the recirculation region downstream of the step.

The calculations were carried out with fluids represented by the sum of a Newtonian solvent contribution and a single-mode Phan-Thien and Tanner polymeric contribution. Although the predicted cat's ears were not as intense as in the experiments, these simulations clearly showed that the near wall peaks required a non-negligible second normal stress difference in combination with high levels of strain hardening of the extensional viscosity, large elastic effects measured by a Deborah number, intermediate levels of inertia and shear thinning. It is not clear at this stage whether the second normal stress difference is a necessary condition or if it just enhances the appearance of the velocity overshoots, but the recent observation of Alves[35] involving the upper convected Maxwell model suggests the latter reason in which case use of this constitutive equation should allow the effect to be seen provided convergence can be achieved. In the extensive parametric investigation of this flow by Afonso

and Pinho[28] with the single mode PTT model, the predicted cat's ears were always much weaker than those seen in these experiments in spite of the wide range of values for parameters ε, ξ and Deborah number tested. Calculations outside the ranges for parameters ε, De, and ξ diverged, an indication of the high Deborah number problem and constitutive instability (for ξ). All this suggests that the use of a multimode PTT model will not, by itself, improve significantly the amplitude of the velocity overshoots (say, by an order of magnitude) and that different constitutive equations are required in order to capture intense velocity overshoots. In this respect, it is also worth mentioning that increasing N_2 in the PTT model, which we found necessary for capturing cat's ears in this particular geometry, leads to constitutive instabilities due to a nonmonotonic behavior of the shear stress[40] and this constitutes another reason for using a different constitutive model, even though they are not responsible for the velocity overshoots as shown by Afonso and Pinho.[28] Capturing the cat's ears certainly also requires an appropriate representation of the transient stress growth of the various rheological properties and this depends not only on the use of a multimode model, but also on the inherent features of a single mode model.

As a future development of this work, we intend to use a different numerical method, such as the log-conformation technique,[41] to see if it is able to provide converged solutions in regions of the $\varepsilon-\xi-De-\beta$ space so far unattained with this flow problem, such as simulations with $\xi=0$ with $\varepsilon<0.005$ and large values of De with and without strong shear-thinning. The next step in trying to predict intense cat's ears in this geometry thus calls in the first instance for the use of the log-conformation technique with the same PTT model and later for the use of other viscoelastic models, especially those that are able to predict second normal stress differences without introducing any unphysical characteristics. In any case, at this stage we do not expect full quantitative agreement with experiments in this complex three-dimensional flow, since the available constitutive models are

not even able to exactly match experiments in simpler two-dimensional flows. A well-known failure in such flows is the simultaneous correct prediction of the flow kinematics and Couette correction in planar and axisymmetric sudden contraction flows.

[1] F. Durst, A. Melling, and J. H. Whitelaw, "Low Reynolds number flow over a plane sudden expansion," J. Fluid Mech. **64**, 111 (1974).

[2] W. Cherdron, F. Durst, and J. H. Whitelaw, "Asymmetric flows and instabilities in symmetric ducts with sudden expansions," J. Fluid Mech. **84**, 13 (1978).

[3] R. M. Fearn, T. Mullin, and K. A. Cliffe, "Nonlinear phenomena in a symmetric sudden expansion," J. Fluid Mech. **211**, 595 (1990).

[4] D. Drikakis, "Bifurcation phenomena in incompressible sudden expansion flows," Phys. Fluids **9**, 76 (1997).

[5] E. Schreck and M. Schafer, "Numerical study of bifurcation in three-dimensional sudden channel expansions," Comput. Fluids **29**, 583 (2000).

[6] R. J. Poole, M. P. Escudier, and P. J. Oliveira, "Laminar flow of a viscoelastic shear-thinning liquid through a plane sudden expansion preceded by a gradual contraction," Proc. R. Soc. London, Ser. A **461**, 3827 (2005).

[7] G. Biswas, M. Breuer, and F. Durst, "Backward-facing step flows for various expansion ratios at low and moderate Reynolds numbers," J. Fluids Eng. **126**, 362 (2004).

[8] H. K. Moffat, "Viscous and resistive eddies near sharp corners," J. Fluid Mech. **18**, 1 (1964).

[9] C. H. Hsu and T. Y. Chou, "Unsteady flow of a second-grade fluid past a backward-facing step," Int. J. Non-Linear Mech. **32**, 947 (1997).

[10] F. J. H. Gijsen, F. N. van de Vosee, and J. D. Janssen, "Wall shear stress in backward-facing step flow of a red blood cell suspension," Biorheology **35**, 263 (1998).

[11] P. Townsend and K. Walters, "Expansion flows of non-Newtonian liquids," Chem. Eng. Sci. **49**, 749 (1994).

[12] N. Phan-Thien and R. I. Tanner, "A new constitutive equation derived from network theory," J. Non-Newtonian Fluid Mech. **2**, 353 (1977).

[13] A. Baloch, P. Townsend, and M. F. Webster, "On vortex development in viscoelastic expansion and contraction flows," J. Non-Newtonian Fluid Mech. **65**, 133 (1996).

[14] K. Lee, M. R. Mackley, T. C. B. McLeish, T. M. Nicholson, and O. G. Harlen, "Experimental observation and numerical simulation of transient 'stress fangs' within flowing molten polyethylene," J. Rheol. **45**, 1261 (2001).

[15] M. P. Escudier and S. E. Smith, "Fully developed turbulent flow of Newtonian liquids through a square duct," Proc. R. Soc. London, Ser. A **457**, 911 (2001).

[16] R. J. Poole and M. P. Escudier, "Turbulent flow of viscoelastic liquids through an axisymmetric sudden expansion," J. Non-Newtonian Fluid Mech. **117**, 25 (2004).

[17] M. P. Escudier, F. Presti, and S. E. Smith, "Drag reduction in the turbulent pipe flow of polymers," J. Non-Newtonian Fluid Mech. **81**, 197 (1999).

[18] K. Walters, A. Q. Bhatti, and N. Mori, *The Influence of Polymer Conformation on the Rheological Properties of Aqueous Polymer Solutions: Recent Developments in Structured Continua*, Pitman Research Notes in Mathematics Series, edited by D. De Kee and P. N. Kaloni (Longman, Essex, 1990), Vol. 2.

[19] K. Yasuda, R. C. Armstrong, and R. E. Cohen, "Shear flow properties of concentrated solutions of linear and star branched polystyrenes," Rheol. Acta **20**, 163 (1981).

[20] M. P. Escudier, I. W. Gouldson, A. S. Pereira, F. T. Pinho, and R. J. Poole, "On the reproducibility of the rheology of shear-thinning liquids," J. Non-Newtonian Fluid Mech. **97**, 99 (2001).

[21] H. A. Barnes, J. F. Hutton, and K. Walters, *An Introduction to Rheology* (Elsevier Science, Amsterdam, 1989).

[22] R. B. Bird, R. C. Armstrong, and O. Hassager, *Dynamics of Polymeric Fluids*, 2nd ed. (Wiley-Interscience, New York, 1987), Vol. 1.

[23] N. Phan-Thien, "A. non-linear network viscoelastic model," J. Rheol. **22**, 259 (1978).

[24] P. J. Oliveira, F. T. Pinho, and G. A. Pinto, "Numerical simulation of nonlinear elastic flows with a general collocated finite-volume method," J. Non-Newtonian Fluid Mech. **79**, 1 (1998).

[25] M. A. Alves, F. T. Pinho, and P. J. Oliveira, "Effect of a high resolution differencing scheme on finite-volume predictions of viscoelastic flows," J. Non-Newtonian Fluid Mech. **93**, 287 (2000).

[26] M. A. Alves, P. J. Oliveira, and F. T. Pinho, "A convergent and universally bounded interpolation scheme for the treatment of advection," Int. J. Numer. Methods Fluids **41**, 47 (2003).

[27] P. H. Gaskell and A. K. C. Lau, "Curvature-compensated convective transport: SMART a new boundedness preserving transport algorithm," Int. J. Numer. Methods Fluids **41**, 617 (1988).

[28] A. Afonso and F. T. Pinho, "Numerical investigation of the velocity overshoots in the flow of viscoelastic fluids inside a smooth contraction," J. Non-Newtonian Fluid Mech. **139**, 1 (2006).

[29] J. A. Wheeler and E. H. Wissler, "Steady flow of non-Newtonian fluids in a square duct," Trans. Soc. Rheol. **10**, 353 (1966).

[30] B. Gervang and P. S. Larsen, "Secondary flows in straight ducts of rectangular cross section," J. Non-Newtonian Fluid Mech. **39**, 217 (1991).

[31] B. Debbaut, T. Avalosse, J. Dooley, and K. Hughes, "On the development of secondary motions in straight channels induced by the second normal stress difference: Experiments and simulations," J. Non-Newtonian Fluid Mech. **69**, 255 (1997).

[32] C. G. Speziale, R. M. C. So, and B. A. Younis, "On the prediction of turbulent secondary flows," in *Near-Wall Turbulent Flows*, edited by R. M. C. So, C. G. Speziale, and B. E. Launder (Elsevier, New York, 1993), pp. 105–114.

[33] S. C. Xue, N. Phan-Thien, and R. I. Tanner, "Numerical study of secondary flows of viscoelastic fluid in straight pipes by an implicit finite volume method," J. Non-Newtonian Fluid Mech. **59**, 191 (1995).

[34] R. J. Poole, M. A. Alves, P. J. Oliveira, and F. T. Pinho, "Plane sudden expansion flows of viscoelastic liquids," J. Non-Newtonian Fluid Mech. **146**, 79 (2007).

[35] M. A. Alves (personal communication, 2006).

[36] M. A. Alves and R. J. Poole, "Divergent flows in contractions," J. Non-Newtonian Fluid Mech. **144**, 140 (2007).

[37] F. T. Pinho, P. J. Oliveira, and J. P. Miranda, "Pressure losses in the laminar flow of shear-thinning power law fluids across a sudden axisymmetric expansion," Int. J. Heat Fluid Flow **24**, 747 (2003).

[38] F. M. White, *Viscous Fluid Flow*, 2nd ed. (McGraw-Hill, New York, 1991).

[39] R. J. Poole, M. P. Escudier, A. Afonso, and F. T. Pinho, "Laminar viscoelastic flow over a backward-facing step," XIVth International Congress on Rheology, Seoul, South Korea (2004), CD-ROM Paper NF-06.

[40] P. Español, X. F. Yuan, and R. C. Ball, "Shear banding flow in the Johnson-Segalman fluid," J. Non-Newtonian Fluid Mech. **65**, 93 (1996).

[41] R. Fattal and R. Kupferman, "Constitutive laws for the matrix-logarithm of the conformation tensor," J. Non-Newtonian Fluid Mech. **123**, 281 (2004).